

# Localized Magnetic States in Graphene

Bruno Uchoa<sup>1</sup>, Valeri N. Kotov<sup>1</sup>, N. M. R. Peres<sup>2</sup>, and A. H. Castro Neto<sup>1</sup>

<sup>1</sup>*Department of Physics, Boston University, 590 Commonwealth Avenue, Boston, MA 02215, USA and*

<sup>2</sup>*Centro de Física e Departamento de Física, Universidade do Minho, P-4710-057, Braga, Portugal*

(Dated: June 21, 2024)

We examine the conditions necessary for the presence of localized magnetic moments on adatoms with inner shell electrons in graphene. We show that the low density of states at the Dirac point, and the anomalous broadening of the adatom electronic level, lead to the formation of magnetic moments for arbitrarily small local charging energy. As a result, we obtain an anomalous scaling of the boundary separating magnetic and non-magnetic states. We show that, unlike any other material, the formation of magnetic moments can be controlled by an electric field effect.

PACS numbers: 73.20.Hb, 81.05.Uw, 73.20.-r, 73.23.-b

Graphene, a two-dimensional (2D) allotrope of carbon, has singular spectroscopic and transport properties [1, 2, 3, 4] due to its unusual electronic excitations described in terms of massless, chiral, “relativistic” Dirac fermions [5]. Besides being a possible test bed for relativistic quantum field theory [6], graphene has a great technological potential due to its structural robustness, allowing extreme miniaturization [7], and a flexible electronic structure that can be controlled by an applied perpendicular electric field [8].

In this paper we show that graphene has also potentiality for *spintronics*, that is, independent control of the charge and the spin of the charge carriers [9]. Unlike diluted magnetically semiconductors (DMS) [10] where the location of the magnetic ions is random and hence unpredictable, adatoms can be positioned in graphene using a scanning tunneling microscope (STM) [11]. Furthermore, as we are going to show, the magnetic properties of adatoms such as size of the magnetic moment and Curie temperatures can be controlled by an external electric field, an effect unparalleled in condensed matter systems.

The basic model for the study of magnetic moment formation in metals is the well-known Anderson impurity model [13]. In this model an ion with inner shell electrons with energy  $\epsilon_0$  hybridizes, via a hopping term of energy  $V$ , with a conduction sea of electrons. While the conduction electrons are described by a Fermi liquid with featureless, essentially constant, density of states (DOS), the impurity ion is assumed to be strongly interacting. The Coulomb energy required for double occupancy of an energy level in the ion is given by  $U$ . Anderson showed that when  $\epsilon_0$  is below the Fermi energy,  $\mu$ , and the energy of the doubly occupied states,  $\epsilon_0 + U$ , is larger than  $\mu$ , a magnetic state is possible if  $U$  is sufficiently large and/or  $V$  sufficiently small.

Here we apply the Anderson model to graphene and show that the energy dependence of the DOS leads to anomalous broadening of the adatom level and strongly favors the formation of local magnetic moments. In particular we show that, unlike the case of ordinary metals, this anomalous broadening allows the formation of magnetic states even when  $\epsilon_0$  is *above* the Fermi energy at relatively small  $U$ . We also find, in contrast with the usual metallic case, an anomalous scaling of

the magnetic boundary separating magnetic and non-magnetic impurity states. Finally, we establish that the local magnetic moments can be mastered by the application of an external gate voltage, leading to a complete control of the magnetic properties of adatoms in graphene.

We consider an impurity atom adsorbed on the surface of the graphene sheet, on top of a carbon (see Fig. 1). The tight-binding Hamiltonian of the electrons in graphene is

$$H_{TB} = -t \sum_{\sigma} \sum_{\langle i,j \rangle} [a_{\sigma}^{\dagger}(\mathbf{R}_i) b_{\sigma}(\mathbf{R}_j) + H.c.], \quad (1)$$

where  $a_{\sigma}(\mathbf{R}_i)$  ( $b_{\sigma}(\mathbf{R}_i)$ ) annihilates and electron with spin  $\sigma = \uparrow, \downarrow$  on sublattice  $A$  ( $B$ ) at position  $\mathbf{R}_i$ ,  $\langle i, j \rangle$  stands for summation over nearest neighbors, and  $t$  ( $\approx 2.7$  eV) is the nearest neighbor hopping energy. In momentum space, we have (we use units such that  $\hbar = 1$ ):

$$H_{TB} = -t \sum_{\mathbf{k}, \sigma} [\phi(\mathbf{k}) a_{\mathbf{k}, \sigma}^{\dagger} b_{\mathbf{k}, \sigma} + \phi^*(\mathbf{k}) b_{\mathbf{k}, \sigma}^{\dagger} a_{\mathbf{k}, \sigma}] \quad (2)$$

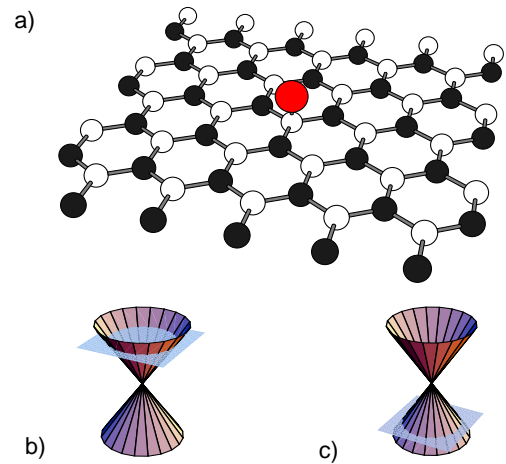


Figure 1: (color on line) (a) Honeycomb lattice with an impurity atom. Black: sublattice A; White: sublattice B. Intersection of the Dirac cone spectrum,  $\epsilon_{\pm}(\mathbf{k}) = \pm v_F k$ , with the localized level spectrum,  $E_f(\mathbf{k}) = \epsilon_0$ : b)  $\epsilon_0 > 0$ ; (c)  $\epsilon_0 < 0$ .

where  $\phi(\mathbf{k}) = \sum_{\vec{\delta}} e^{i\mathbf{k}\cdot\vec{\delta}}$ , with  $\vec{\delta}_1 = a(\hat{x}/2 + \sqrt{3}/2\hat{y})$ ,  $\vec{\delta}_2 = a(\hat{x}/2 - \sqrt{3}/2\hat{y})$  and  $\vec{\delta}_3 = -a\hat{x}$  are the nearest neighbor vectors. Diagonalization of the Hamiltonian (2) generates two bands,  $\epsilon_{\pm}(\mathbf{k}) = \pm t|\phi(\mathbf{k})|$ , which can be linearized around the Dirac points  $\mathbf{Q}$  at the corners of the Brillouin zone:  $\epsilon_{\pm}(\mathbf{Q} + \mathbf{q}) \approx \pm v_F|\mathbf{q}|$ , where  $v_F = 3ta/2$  ( $\approx 10^6$  m/s) is the Fermi velocity of the Dirac electrons.

The hybridization with the localized orbital of the impurity atom on a given site, say, on sublattice  $B$ , is given by:  $H_V = V \sum_{\sigma} [f_{\sigma}^{\dagger} b_{\sigma}(0) + H.c.]$ , where  $f_{\sigma}$  ( $f_{\sigma}^{\dagger}$ ) annihilates (creates) an electron with spin  $\sigma = \uparrow, \downarrow$  at the impurity. In momentum space we have:

$$H_V = V/\sqrt{N_b} \sum_{\mathbf{p}, \sigma} (f_{\sigma}^{\dagger} b_{\mathbf{p}, \sigma} + b_{\mathbf{p}, \sigma}^{\dagger} f_{\sigma}), \quad (3)$$

where  $N_b$  is the number of sites on sublattice  $B$  contained in the expanded unit cell of graphene with the impurity.

The Hamiltonian of the localized orbital is described by a single level,  $H_f = \epsilon_0 \sum_{\sigma} f_{\sigma}^{\dagger} f_{\sigma}$ . The electronic correlations in the inner shell states can be described by a Hubbard-like term:  $H_U = U f_{\uparrow}^{\dagger} f_{\uparrow} f_{\downarrow}^{\dagger} f_{\downarrow}$ . Following Anderson, we use a mean-field decoupling of the interaction,  $H_U \rightarrow \sum_{\sigma} U n_{-\sigma} f_{\sigma}^{\dagger} f_{\sigma} - U n_{\uparrow} n_{\downarrow}$ , where  $n_{\sigma} = \langle f_{\sigma}^{\dagger} f_{\sigma} \rangle$  is the occupation for each of the two spin states. The Hubbard term can be absorbed into the definition of the local impurity energy,  $H_f = \sum_{\sigma} \epsilon_{\sigma} f_{\sigma}^{\dagger} f_{\sigma}$ , where  $\epsilon_{\sigma} = \epsilon_0 + U n_{-\sigma}$  is the energy of the localized electrons in a given spin state in the presence of a local charging energy  $U$ .

The formation of a magnetic moment is determined by the occupation of the two spin states at the impurity,  $n_{\sigma}$ . A localized moment forms whenever  $n_{\uparrow} \neq n_{\downarrow}$ . The determination of  $n_{\sigma}$  requires the self-consistent calculation of the density of states at the impurity level,  $\rho_{ff}(\omega)$ , which incorporates the broadening of the impurity level due to hybridization with the bath of electrons in graphene. The occupation of the impurity level is given by:

$$n_{\sigma} = \int_{-\infty}^{\mu} d\omega \rho_{ff, \sigma}(\omega). \quad (4)$$

The Green's function of  $f$ -electrons is:  $G_{ff, \sigma}(t) = -i\langle T [f_{\sigma}(t) f_{\sigma}^{\dagger}(0)] \rangle$ , and its retarded part can be written as:

$$G_{ff, \sigma}^R(\omega) = [\omega - \epsilon_{\sigma} - \Sigma_{ff}^R(\omega) + i0^+]^{-1}, \quad (5)$$

where

$$\Sigma_{ff}^R(\omega) = V^2/N_b \sum_{\mathbf{p}} G_{bb, \sigma}^0(\mathbf{p}, \omega), \quad (6)$$

is the self-energy of the  $f$ -electrons, which is defined in terms of the non-interacting Green's function of the graphene electrons in a given sublattice,  $G_{bb, \sigma}^0(\mathbf{p}, t) = -i\langle T [b_{\sigma\mathbf{p}}(t) b_{\sigma\mathbf{p}}^{\dagger}(0)] \rangle_0$ :

$$G_{bb, \sigma}^0(\mathbf{p}, \omega) = \omega/(\omega^2 - v_F^2|\mathbf{p}|^2 + i0^+ \text{sign}(\omega)). \quad (7)$$

In this case (6) becomes:

$$\Sigma_{ff}^R(\omega) = -V^2 \frac{\omega}{D^2} \ln \left( \frac{|\omega^2 - D^2|}{\omega^2} \right) - iV^2 \frac{\pi|\omega|}{D^2} \theta(D - |\omega|), \quad (8)$$

where  $D$  is a high-energy cut-off of the order of the graphene bandwidth ( $D \approx 7$  eV).

The real part of  $\Sigma_{ff}^R(\omega)$  defines the quasiparticle residue  $Z^{-1}(\omega) = 1 + (V^2/D^2) \ln(|D^2 - \omega^2|/\omega^2)$  of the  $f$ -electrons, while the imaginary part gives the broadening of the localized level due to the hybridization. As expected, the anomalous character of the problem is explicitly manifested in the linear dependence of the broadening with the energy, which is proportional to the electronic DOS in graphene. Furthermore, notice that  $Z(\omega)$  vanishes at  $\omega \rightarrow 0$ . Replacing Eq. (8) into Eq. (5) gives the density of states of the localized level,  $\rho_{ff, \sigma}(\omega) = -1/\pi \text{Im} G_{ff, \sigma}^R(\omega)$ :

$$\rho_{ff, \sigma}(\omega) = \frac{1}{\pi} \frac{\Delta|\omega| \theta(D - |\omega|)}{[Z^{-1}(\omega) \omega - \epsilon_{\sigma}]^2 + \Delta^2 \omega^2} \quad (9)$$

where  $\Delta = \pi V^2/D^2$  is the dimensionless hybridization.

Notice that, unlike the case of impurities in metals, the impurity density of states is not a simple lorentzian. The impurity DOS, (9), is peaked around the quasiparticle pole at  $\epsilon_{\sigma} = 0$  and  $\omega \rightarrow 0$ . We can expand  $Z(\omega)$  around the singularity at  $\omega_0 Z^{-1}(\omega_0) \sim \epsilon_{\sigma}$  for  $\omega_0 \rightarrow 0$ , where we may approximate  $Z(\omega_0) \sim Z(\epsilon_{\sigma})$  except for a double-logarithmic corrections that can be safely ignored [14]. The anomalous broadening gives rise to a logarithmic divergence in the ultraviolet when the DOS of the level is integrated in (4),

$$n_{\sigma} = \frac{Z_{\sigma}^{-1}}{(Z_{\sigma}^{-2} + \Delta^2)} \left[ \theta(\mu - \epsilon_{\sigma}) + \frac{1}{\pi} \arctan \left( \frac{|\mu| \Delta}{\epsilon_{\sigma} - \mu} \right) + \Theta_{\sigma} \right], \quad (10)$$

where for brevity  $Z(\epsilon_{\sigma}) \equiv Z_{\sigma}$ . The term  $\Theta_{\sigma}$  contains the contribution coming from the cut-off regularization:

$$\Theta_{\sigma} = Z_{\sigma} \frac{\Delta}{\pi} \ln \left[ \frac{W_{\sigma}(E_{\sigma})^{\gamma}}{(\epsilon_{\sigma})^{1+\gamma}} \right] - \frac{1}{\pi} \arctan \left( \frac{\Delta D}{D Z_{\sigma}^{-1} + \epsilon_{\sigma}} \right), \quad (11)$$

where  $\gamma = \text{sign}(\mu)$ , and

$$E_{\sigma} = \sqrt{(\epsilon_{\sigma} - \mu Z_{\sigma}^{-1})^2 + \mu^2 \Delta^2} \quad (12)$$

$$W_{\sigma} = \sqrt{(D Z_{\sigma}^{-1} + \epsilon_{\sigma})^2 + D^2 \Delta^2}. \quad (13)$$

In Fig. 2 we show the boundary between magnetic and non-magnetic impurity states as a function of the parameters  $x = D\Delta/U$  and  $y = (\mu - \epsilon_0)/U$ . Notice that the magnetic boundary is not symmetric between the cases where the impurity is above ( $\epsilon_0 > 0$ ) or below ( $\epsilon_0 < 0$ ) the Dirac point. Moreover, unlike the metallic problem [13] the boundary is not symmetric around  $y = 0.5$ . This reflects the particle-hole symmetry breaking due to the presence of the localized level. In the case where  $\epsilon_0 > 0$  (see Fig. 2a), the magnetic boundary crosses the line  $y = 0$ , and the level magnetizes even when

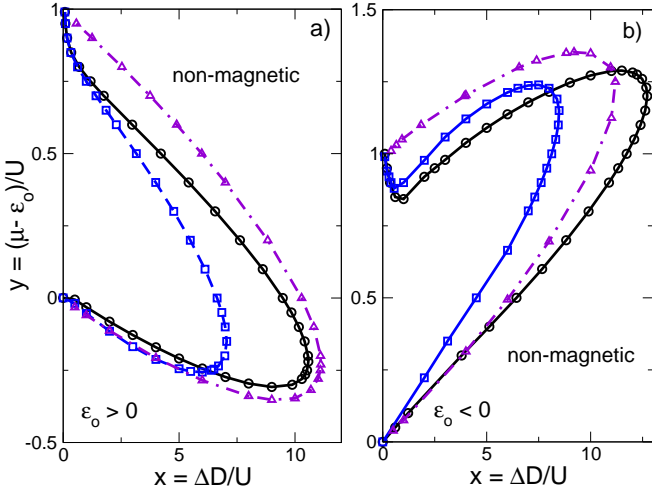


Figure 2: Boundary between magnetic and non-magnetic impurity states in the scaling variables  $x$  and  $y$  for  $\epsilon_0 > 0$  (a) and  $\epsilon_0 < 0$  (b). Circles:  $|\epsilon_0|/D = 0.029$ ,  $V/D = 0.14$ ; Squares:  $\epsilon_0/D = 0.043$  and  $V/D = 0.14$ ; Triangles:  $|\epsilon_0|/D = 0.029$ ,  $V/D = 0.03$ . The upturn close to  $y = 1$  and  $x \rightarrow 0$  on panel b) is not visible in this scale when  $V$  is very small (triangles). See details in the text.

the impurity is above the Fermi energy. This is understood by the fact that the hybridization leads to a large broadening of the impurity level density of states (with a tail that decays like  $1/\omega$ ) that crosses the Fermi energy even when the bare level energy is above it. In the opposite case of  $\epsilon_0 < 0$  a similar effect occurs with the crossing of the magnetic boundary along the  $y = 1$  line, something that also does not occur in ordinary metals [12]. This implies even when the energy of the doubly occupied state is below the Fermi level ( $\epsilon_0 + U < \mu$ ), because of the large broadening, the impurity magnetizes if  $U$  is not too large or too small. The up turn close to  $y = 1$  and  $x \ll 1$  in the  $\epsilon_0 < 0$  case only reflects that in this limit ( $U, \mu \gg \epsilon_0$ , for finite  $\epsilon_0$ ) the physics of the Dirac points is irrelevant and we recover the usual Anderson model in ordinary metals, where the transition curve approaches the point  $x = 0, y = 1$  from below [13].

The dependence of the scaling of the magnetic boundary with  $\epsilon_0$  and  $\Delta$  (see Fig. 2) shows that the size of the magnetic region grows as  $|\epsilon_0|$  approaches the energy of the Dirac points. In this situation the DOS around the localized level is suppressed, favoring the formation of a local magnetic moment. In particular, in the limit where the level is nearly at the Dirac point ( $|\epsilon_0| \rightarrow 0$ ), the level nearly decouples from the bath and the impurity can magnetize in principle for any small finite charging energy  $U$ . On the other hand, the magnetic region shrinks in the  $y$  direction as the hybridization parameter  $\Delta$  grows (see Fig.2). In the limit of  $\Delta \rightarrow 0$  and  $U$  finite a local magnetic moment forms whenever  $0 < y < 1$ , as in the case of an impurity in a metal.

The application of a potential  $V_g$  through an electric field via a back gate [1] shifts the chemical potential  $\mu$  and moves the magnetic state of the impurity in the vertical direction ( $y$ )

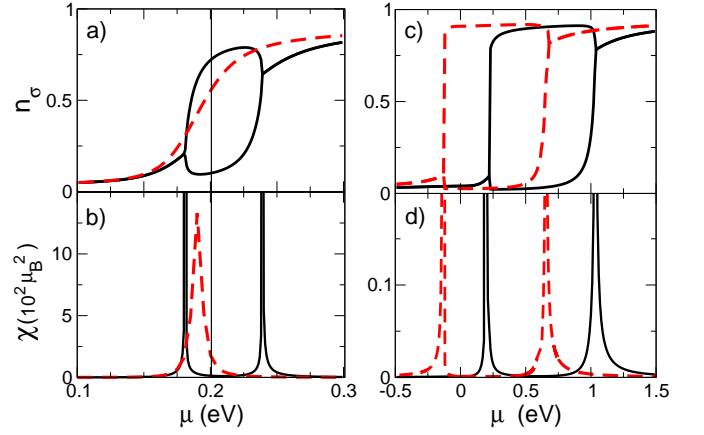


Figure 3: (color on line)  $n_\uparrow(\mu), n_\downarrow(\mu)$  and  $\chi(\mu)$  for  $|\epsilon_0|/D = 0.029$  and  $V/D = 0.14$  ( $D \sim 7$  eV). Left panels:  $x = 11$  (dashed curves), and  $x = 5$  (solid). The impurity magnetizes inside the bubble ( $n_\uparrow \neq n_\downarrow$ ). The vertical line marks the position of the level,  $\epsilon_0 = 0.2$  eV. On the right: Comparison between  $\epsilon_0 = 0.2$  eV (solid) and  $\epsilon_0 = -0.2$  eV (dashed) at  $x = 0.45$ .

in Fig. 2. We assume that  $x = D\Delta/U$  does not change much with applied voltage, even with screening coming from a finite Fermi energy. Hence, the magnetization of the impurity can in principle be turned on and off, depending only on the gate voltage applied to graphene. This is better illustrated by looking at the behavior of the impurity magnetic susceptibility. In the presence of a field, the energy of the impurity spin states changes to  $\epsilon_\sigma = \epsilon_0 - \sigma\mu_B B + Un_{-\sigma}$ . In the zero field limit, the magnetic susceptibility of the impurity,  $\chi = \mu_B \sum_\sigma \sigma (dn_\sigma/dB)_{B=0}$  ( $\mu_B$  is the Bohr magneton, and  $B$  is a small applied magnetic field), can be calculated straightforwardly from Eq. (10):

$$\chi = -\mu_B^2 \sum_{\sigma=\uparrow\downarrow} \frac{dn_\sigma}{d\epsilon_\sigma} \cdot \frac{1 - U \frac{dn_{-\sigma}}{d\epsilon_{-\sigma}}}{1 - U^2 \frac{dn_{-\sigma}}{d\epsilon_{-\sigma}} \frac{dn_\sigma}{d\epsilon_\sigma}}. \quad (14)$$

In the lower panels of Fig. 3 we show  $\chi(\mu)$  for  $\epsilon_0 = 0.2$  eV,  $V \sim 1$  eV and  $D \sim 7$  eV, for different values of  $x$ . The corresponding magnetization line for this set of parameters is defined by the solid curve with black circles in Fig. 2a. While the impurity remains non-magnetic for any  $y$  at  $x = 11$  ( $U \sim 40$  meV), as shown in Fig. 2a, the impurity state already crosses the magnetic boundary twice for  $x = 5$ , where  $U$  is nearly twice larger. In this case, a large magnetic moment of  $\sim 0.5 \mu_B$  forms below the energy of the level, at  $\mu \sim 0.18$  eV (see Fig. 3a and 3b). At  $x = 0.45$  ( $U = 1$  eV), the local moment exists for very large  $\mu \sim 1$  eV, and a strong and uniform magnetic moment of  $\sim 0.9 \mu_B$  forms in almost the whole magnetic region (see Fig. 3c). A similar qualitative behavior for the magnetization occurs when  $\epsilon_0 < 0$  (Fig. 3c,d). As  $U$  becomes large ( $> 1$  eV), the magnetic transition becomes very sharp. For  $\epsilon_0 \sim 0.5$  eV and  $V = 1$  eV, the impurity in graphene can magnetize for  $U \gtrsim 0.1$  eV. While the local charging energy  $U$  for transition metals in a metallic matrix is of the order of  $\sim 5-10$  eV [17], in graphene, where the

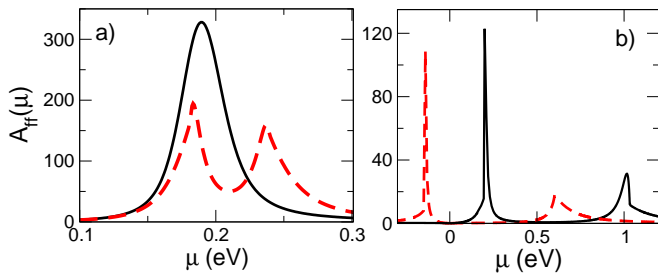


Figure 4: (color on line) Spectral function (in units of  $1/\text{eV}$ ) of the  $f$ -electrons at the Fermi energy  $\mu$  for  $|\epsilon_0|/D = 0.029$  and  $V/D = 0.14$  ( $D \sim 7$  eV). (a)  $x = 11$  (solid curve) and  $x = 5$  (dashed) for  $\epsilon_0 > 0$  (see Fig. 2). (b)  $x = 0.45$  for  $\epsilon_0 > 0$  (solid) and  $\epsilon_0 < 0$  (dashed).

effective hybridization can be large due to the linear increase of the DOS, the critical  $U$  for magnetization of the impurity can be much smaller. Hence, transition elements that usually do not magnetize when introduced in ordinary metals, can actually become magnetic in graphene. Indeed, the tendency to formation of local magnetic moments has been noticed by *ab initio* calculations with transition metal adatoms [15] and molecules [16] adsorbed in graphene.

In order to show that the spectroscopic functions of the magnetic impurities can also be controlled by electric field effect we show, in Fig. 4, the spectral function of the localized electrons calculated at the Fermi energy:  $A_{ff}(\omega = \mu) = 2\pi \sum_{\sigma} \rho_{ff,\sigma}(\mu)$ . Differently from the usual metallic case, the spectral weight is not equally distributed between the two peaks, which are located around the level and at the reentrant magnetic transition, near  $\mu \sim \epsilon_0 + U$ . The solid line in Fig. 4a is a non-magnetic resonance in a situation where the impurity state does not cross the magnetic boundary of the scaling diagram by changing  $y(\mu)$  for some fixed  $x$ . In the other curves of Fig. 4, the energy splitting of the peaks scales with  $U$  and the position of the peaks coincides with the jump in the susceptibility shown in Fig. 3.

The dependence of the impurity density of states with  $\mu$ , and hence with gate bias, allows for the identification of the formation of local moments through ordinary transport measurements. For finite  $\mu$ , the hybridization of the itinerant electrons with the localized level renormalizes the charge scattering channels and hence the carrier conductivity,  $\sigma = 2e^2\mu\tau$ , where  $\tau^{-1}$  is the impurity scattering rate. Second order perturbation theory gives [17]:

$$\tau^{-1} - \tau_0^{-1} \propto n_0 V^2 A_{ff}(\mu), \quad (15)$$

where  $\tau_0^{-1}$  is the scattering rate of the electrons in the absence of impurities and  $n_0$  is the impurity concentration. In the limit of very large  $U$ , however, the scattering is dominated by the spin flip channels in the Kondo regime [18, 19, 20, 21, 22]. When the position of the level is located in the experimental range accessible by the application of a gate voltage  $\sim -0.3$  to  $0.3$  eV [1], the shape of the dip in the conductivity produced by the impurity scattering can indicate not only the position of

the level but also the presence of local magnetic moments (notice that the non-magnetic resonance in the spectral function is quite symmetric).

In the presence of a finite density of magnetic moments a macroscopic magnetic state can emerge due to the RKKY interaction between them. At the Dirac point ( $\mu = 0$ ) the interaction is purely ferromagnetic due to the vanishing of the Fermi wavevector,  $k_F = \mu/v_F$  [23]. However, at finite bias voltage the RKKY interactions display  $2k_F$  oscillations decaying like  $1/r^3$  [24] that can couple the magnetic moments ferromagnetically or anti-ferromagnetically depending on the position and geometry of the adatom lattice (that can be conveniently chosen using a STM). Hence, by changing the bias voltage a variety of different macroscopic magnetic states can emerge.

In conclusion, we have examined the conditions under which a transition metal adatom on graphene can form a local magnetic moment. We find that due to the anomalous broadening of the adatom local electronic states, moment formation is much easier in graphene. Furthermore, the magnetic properties of adatoms can be controlled by electric field effect allowing for the possibility of using graphene in spintronics. We thank V. M. Pereira, J. M. B. Lopes dos Santos, A. Polkovnikov, and S. W. Tsai for helpful discussions. NMRP acknowledge the financial support from POCI 2010 via project PTDC/FIS/64404/2006. BU acknowledges CNPq, Brazil, for the support under the grant 201007/2005-3.

- 
- [1] K. S. Novoselov *et al.*, Science **306**, 666 (2004).
  - [2] K. S. Novoselov *et al.*, Nature **438**, 197 (2005).
  - [3] Y. Zhang *et al.*, Nature **438**, 201 (2005).
  - [4] A. K. Geim, and K. S. Novoselov, Nat. Mat. **6**, 183 (2007).
  - [5] A. H. Castro Neto *et al.*, arXiv:0709.1163.
  - [6] A. H. Castro Neto *et al.*, Physics World **19**, 33 (2006).
  - [7] L. A. Ponomarenko *et al.*, arXiv:0801.0160.
  - [8] E. V. Castro *et al.*, Phys. Rev. Lett. **99**, 216802 (2007).
  - [9] S. A. Wolf *et al.*, Nature **204**, 1488 (2001).
  - [10] See, A. H. MacDonald *et al.*, Nat. Mat. **4**, 195 (2005), and references therein.
  - [11] D. M. Eigler, and E. K. Schweizer, Nature **344**, 524 (1990).
  - [12] A single crossing at  $y = 1$  was found in a chiral Luttinger liquid. See P. Phillips *et al.*, Phys. Rev. B **53**, R468 (1996).
  - [13] P. W. Anderson, Phys. Rev. **124**, 41 (1961).
  - [14] The approximation on  $Z(\omega)$  leads to a deviation of  $\sim 1\%$  from the exact numerical calculation in the scaling diagram.
  - [15] D. M. Duffy, and J. A. Blackman, Phys. Rev. B **58**, 7443 (1998).
  - [16] O. Leenaerts *et al.*, arXiv:0710.1757v1.
  - [17] G. D. Mahan, *Many particle physics* (Plenum, 2000) 3rd ed.
  - [18] D. Withoff and E. Fradkin, Phys. Rev. Lett. **64**, 1835 (1990).
  - [19] G.-M. Zhang *et al.*, Phys. Rev. Lett. **86**, 704 (2001).
  - [20] M. Hentchel, and F. Guinea, Phys. Rev. B **76**, 115407 (2007).
  - [21] B. Dóra, and P. Thalmeier, Phys. Rev. B **76**, 115435 (2007).
  - [22] K. Sengupta and G. Baskaran, arXiv:0705.0257.
  - [23] M. A. H. Vozmediano *et al.*, Phys. Rev. B **72**, 155121 (2005).
  - [24] V. V. Cheianov and V. I. Fal'ko, Phys. Rev. Lett. **97**, 226801 (2006).